PHILIPPINE ENGINEERING JOURNAL
PEJ 2004; **Vol. 25 No. 2**:73–90

Slope Failures Triggered by Heavy Rainfall

Rolando P. Orense*

Department of Civil Engineering
Yamaguchi University Tokiwadai
Ube-shi 755-8611 JAPAN

ABSTRACT

Landslides occur frequently during or following periods of heavy rainfall. This is illustrated by the large-scale landslides and debris flows in Quezon Province which were triggered by a series of typhoons and tropical storms last November-December 2004. In order to understand the mechanism and conditions leading to these slope failures, a comprehensive testing program consisting of constant shear stress drained triaxial tests and model slope experiments was performed using sandy materials obtained from a former landslide site in Japan. Results of both element tests and model experiments clearly showed that slope failure is induced due to the development of pore-water pressure in slope. As soil moisture contents within the slope approach critical values, ground deformations are mobilized. Therefore, by properly selecting regions where soil moisture contents must be monitored, possibly in areas where seepage forces will develop, failure initiation in slopes can be predicted. Based on this, a simple monitoring scheme to predict in real-time the occurrence of failures in critical slopes was proposed.

1. INTRODUCTION

Landslides induced by heavy rainfall often occur in marginally stable slopes that consist of various types of soil, such as colluvial and residual soils. Because of its frequency and proximity to various infrastructure developments in landslide-prone areas, rainfall-induced slope instability is considered one of the most significant geo-environmental hazards.

Mitigation of damage caused by rainfall-induced slope failures can be classified broadly in two categories: hard-type approaches, such as slope stabilization methods as in the use of retaining walls, dewatering techniques, anchor piles, etc. and soft-type approaches, such as implementing appropriate alarm and warning systems. Considering the extent of potentially unstable slopes, the first category may not always be feasible due to financial and environmental constraints. Monitoring systems therefore offer viable alternatives. In some locations, e.g. Hong Kong (Brand et al., [1]), the San Francisco Bay area (Keefer et al., [2]), Honolulu (Wilson et al., [3], and Japan (Okada and Sugiyama, [4]), warning systems have been established to help minimize risk. These warning systems, which are based on correlation between rainfall intensity

*Correspondence to: Department of Civil Engineering, Yamaguchi University, Tokiwadai, Ube-shi 755-8611 Japan. email:orense@yamaguchi-u.ac.jp

Received August 2, 2005
Revised October 10, 2005
Accepted November 2, 2005

and frequency of landslides, are highly empirical. They do not take into account the response of the ground during the infiltration process itself, i.e., changes within the soil state which are directly related to landslides, such as degree of saturation, pore pressure and deformation, are not considered.

The mechanism leading to rainfall-induced slope failures can be summarized in general terms as follows. When rainwater infiltrates a soil profile that is initially in an unsaturated state, a decrease in negative pore pressure (or matric suction) occurs. This causes a decrease in the effective normal stress acting along the potential failure plane, which in turn diminishes the available shear strength to a point where equilibrium can no longer be sustained in the slope.

In this paper, slope failures in Quezon Province triggered by heavy rainfall during the passage of a series of typhoons on November-December 2004 are presented to highlight the importance of understanding the mechanism of rainfall-induced slope failures. Moreover, the results of a comprehensive testing program which was carried out in the laboratory to investigate the factors affecting initiation of rainfall-induced landslides are presented. Based on the results of these tests, a simple methodology was proposed to predict in real-time the occurrence of failures in critical slopes and to determine if the failed portion of slope mass would impact important facilities located near the bottom of the slope.

2. EXAMPLE OF RAINFALL-INDUCED LANDSLIDES: THE DECEMBER 2004 SLOPE DISASTERS IN QUEZON PROVINCE

A series of typhoons and tropical storms struck Luzon Island from mid-November to early December 2004 and caused extensive disaster, especially in the eastern coast of the island. The number of death and missing exceeded 1600, and the cost of damage was estimated at US$78.2M. The province of Quezon, located on the eastern side of the Sierra Madre mountain range, was the most severely damaged due to landslides, debris flows and flash floods induced by the heavy rainfall. The affected region is indicated in Figure 1. Hardest hit were the towns of Real, Infanta and General Nakar. More than half of the casualties occurred in these three towns. In addition, damage to civil engineering structures was also extensive, with numerous houses and several bridges washed away by the moving debris and flashfloods. Records obtained by PAGASA (Philippine Atmospheric Geophysical and Astronomical Services Administration) rain gauge in Infanta showed that in the morning of November 29 during the passage of storm Winnie, 342 mm of rain fell during a 9-hr period in Infanta station, after which no more rainfall data was available because floods washed away the rain gauge. According to PAGASA records from 1951-2002, the average annual precipitation in Infanta is about 4016 mm while the average monthly rainfall during the rainy season (Oct-Dec) is 610 mm. These indicate that about 30% of the average annual precipitation and about twice the average monthly precipitation fell within this 2-1/2-week period. Considering the studies made by the National Water Information Network (NWIN), this rainfall event corresponds to one with a return period in the order of 100 years (Orense et al., [6]). Such torrential downpours over the eastern slopes of the mountainous and hilly terrain in eastern Luzon led to massive mudslides and flash floods and accounted for the greatest loss of life.

Aerial reconnaissance works showed that numerous landslides occurred in the southeastern part of Sierra Madre, even in areas which were heavily forested. Trees were uprooted from these mountains and slid down the slopes together with great masses of soils. Most of the

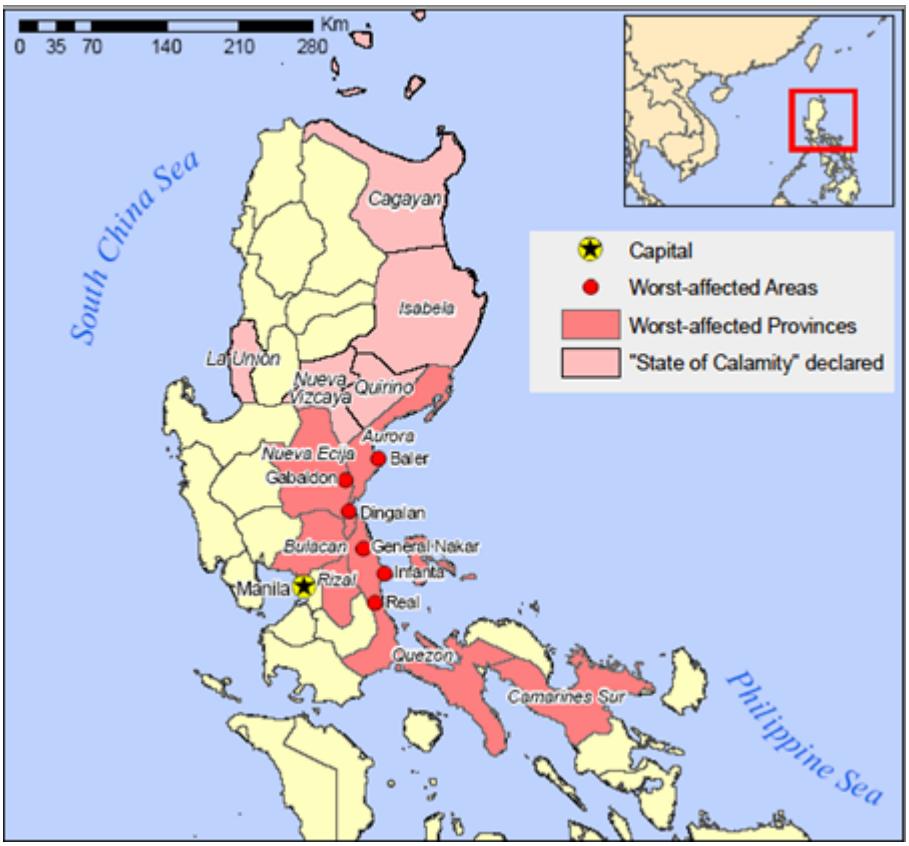

Figure 1. Areas affected by the heavy rainfall which occurred on November - December 2004 (modified from OCHA, [5])

landslides involved only surficial soils and were not deep-seated. Rockslides and rockfalls were also observed near mountain streams. In one of the worst hit areas in Real town, about 100 persons were trapped when a three-storey building being used as an evacuation site collapsed under the impact of one landslide. The site is shown in Figure 2. Moreover, five road bridges were destroyed by the sediment- and debris-laden flood waters, and logs and debris blocked major portions of the national highway, rendering Real and adjacent towns inaccessible to traffic for several weeks. One of the washed-out bridges is shown in Figure 3. In the aftermath of the disaster, government officials blamed the logging activities in the southeastern portion of Sierra Madre mountain ranges as the main cause of landslides and floods in the affected areas. However, aerial photos showed that in the southwestern portion of the mountain ranges, which have almost similar geologic and topographic features, very few landslides occurred although forest cover was very little. Further inspection reveals that landslides were prevalent in steep slopes, whether forested or not. The results of preliminary investigations (Orense et al., [6]) suggest that the heavy rainfall preceding the disaster is the main cause of the slides. Samples obtained in Real and Infanta indicate that the soils in the affected are silty sand and sandy

Figure 2. View of landslide in Real town where more than 100 people were killed

silt, with very few clay content (< 11%). The heavy rainfall saturated the slopes, leading to loss in shear strength and resulted in failures. The existence of highly fractured rocks, steep slopes and thick soil cover also contributed to the mobilization of slope failures. Environmental conditions, particularly land use and logging, were not the main cause of the landslides, but may have contributed to the impact and scale of the disaster.

The case study presented above highlights the significance of increase in soil moisture content associated with rainwater infiltration in inducing slope failure. Fukouka [7] stressed that to analyze the stability of slopes during rainfall, it is necessary to know the change in the saturation ratio and the strength parameters of highly saturated soils.

To study this in detail, a comprehensive testing program was carried out in the laboratory to investigate the process leading to rainfall-induced slope failures and to clarify the parameters essential to initiate failure. Constant shear stress drained triaxial tests on initially unsaturated sandy specimens were conducted to simulate the stress path followed by soil element in a slope during rainfall. Note that since the soils in Quezon are generally sandy silt and silty sand in nature, tests on sandy soils obtained from a natural slope in Japan which also underwent rain-induced collapse are deemed suitable. In these tests, total normal stress and shear stress essentially remained constant during the process of rainwater infiltration. In addition to pore-water pressure inside the specimen, axial and volumetric strains during water infiltration were examined. Moreover, seepage and rainfall tests on instrumented small-scale model slopes were also performed. Pore-water pressure, slope deformation and soil moisture contents at specified points within the slope were monitored.

Figure 3. Real Bridge washed out by the flash floods and debris flows (Photo by E. Billedo)

3. EXPERIMENTAL SET-UP

3.1. Materials Used

The materials employed in both laboratory triaxial and model tests were obtained from Omigawa, Chiba Prefecture (Japan), site of more than 250 landslides associated with the passage of Typhoon No. 25 in September 1971 (Chiba Prefecture, [8]). The materials were generally sandy in nature, and the physical properties are summarized in Table I.

3.2. Constant Shear Stress Drained Tests

The change in stress within a soil element in the field as a result of the hydrologic response of soil during rainfall is referred to in this paper as the field stress path. Consider a soil element on a potential failure plane in a slope subjected to rainwater infiltration. Figure 4 illustrates the Mohr circles representing the corresponding field stress conditions and the stress path followed by such soil element. When the soil element is in an unsaturated state, it has negative pore water pressure (soil suction), as represented by Mohr Circle A. With the infiltration of rainwater into the soil profile, the soil suction dissipates as the soil element becomes saturated. Mohr Circle A migrates from right to left, as shown by Circle B. However, the dissipation of suction by infiltrating rainwater in itself may not lead to failure and generation of positive pore water pressure may be required for failure to take place (Johnson and Sitar, [9]; Sitar et al., [10]; Eckersley, [11]), as represented by Circle C. This implies that at the time of failure,

Property	Value
Specific Gravity, G_s	2.67
Mean grain size, D_{50} (mm)	0.49
Gravel content, (%)	0.5
Sand content (%)	90.1
Fine content (%)	9.4
Coefficient of uniformity C_u	6.47
Coefficient of gradation C_c	1.70
Maximum void ratio, e_{max}	1.07
Minimum void ratio, e_{min}	0.71
Plasticity index I_p	NP

Table I. Properties of Omigawa sand

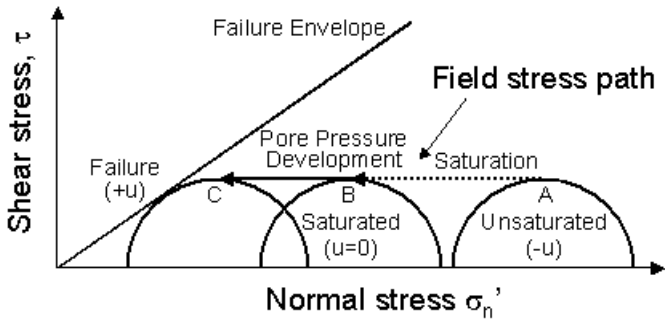

Figure 4. Field stress path in a slope subjected to rainwater infiltration

the soil element along the potential failure plane is nearly saturated and any increase in the bulk unit weight of the soil due to saturation is negligible. In other words, the field stress path followed by a soil element during rainfall is characterized by pore pressure increase at almost constant shear stress condition, as depicted by the horizontal line in Figure 4. The field stress path followed by an unsaturated soil element as described above can be simulated in the laboratory through constant shear stress drained triaxial tests. In the tests, the normal stress, σ'_n, and the shear stress, τ, essentially remain constant during the process of rainwater infiltration (Brand, [12]; Brenner et al., [13]). Consequently, the failure of the slope is primarily caused by a reduction in the matric suction.

In the element tests, an automated stress-controlled triaxial test apparatus was employed. It is equipped with a high air-entry value (300 kPa) ceramic disk at the bottom to measure initial suction of the unsaturated specimen. The soil specimen, 155 mm high and 75 mm in diameter, was prepared on top of the saturated ceramic disk by wet tamping method at specified initial relative density, D_r, and initial moisture content, w. A 12 mm-long pore-water pressure transducer was placed at one-third height of the specimen to monitor changes in pore-water pressure, u. The specimen was first isotropically consolidated and then axial stress was increased to a specified level of principal stress ratio ($K = \sigma_1/\sigma_3$) to represent

field consolidation state of in-situ soil along a potential failure plane. Because typical depths of failure in actual slopes are quite shallow, testing was conducted at low effective confining pressure ($\sigma_3 = 15 \sim 50$ kPa). After full consolidation, water was slowly infiltrated through the bottom ceramic disk until the specimen failed.

During water infiltration, radial and axial deformations of the specimen were continuously monitored using clip gages and linear variable displacement transducer (LVDT), respectively, while axial stress was kept constant by a computer. Moreover, the top cap was vented to the atmosphere, implicitly assuming that pore-air pressure within the specimen remained zero. Furthermore, volume of water entering and leaving the sample was also carefully measured. Detailed discussions of the experimental procedure are given by Farooq et al., [14].

3.3. Small- scale Model Experiments

To supplement the triaxial test results and to observe general failure pattern of slopes during rainfall, a series of model slope tests was performed. The soil box employed is 220 cm long, 80 cm wide and 100 cm high (see Figure 5).Its walls are made of steel plates, except for the front side which is made of transparent acrylic glass for observing the deformation process. The model slopes were constructed in the center portion of the box by laying out Omigawa sand (initial w=10%) in series of horizontal layers, where each layer was tamped equally to achieve a prescribed density. Pore-water pressure meters, soil moisture content transducers (Amplitude Domain Reflectometry or ADR-type) and a shear displacement transducer were installed within the model slope. In addition, pin markers were set on the slope surface as well as on the side adjacent to the acrylic glass wall to examine ground displacements using two video cameras set-up at strategic locations. For further details of the experimental procedure, refer to Shimoma et al., [15] and Orense et al., [16].

In the tests, a failure was initiated in the small-scale model slope either through seepage from water supply chamber located upslope (as shown in Figure 5 to simulate percolating water from upslope in natural ground during rainfall) or through seepage by artificial rainfall using hoses and nozzles. Because of scale effects, it is worthy to mention that the tests were conducted to investigate the general behavior of slopes and were not meant to simulate in-situ conditions.

4. TEST RESULTS AND DISCUSSIONS

4.1. Element Tests

In the experimental program, effects of various parameters related to the initial condition of the specimen were investigated. These parameters include initial relative density, D_r; initial principal stress ratio, K; initial degree of saturation, S_r; initial confining pressure, σ_3; and infiltration rate, Q. Due to space limitation, only limited test results are discussed here. Other test results are presented elsewhere (Farooq et al., [14]). Figure 6 shows the results of constant shear stress drained tests on initially unsaturated samples (initial S_r=20%) in which initial conditions of K=2.5 and σ_3 =25 kPa were kept constant, while D_r was varied from $41 \sim 79\%$. Values of over-all S_r shown in the figure refer to the average within the whole specimen. Notice from Figure 6(a) that there was continuous but gradual development of axial strain, ϵ_a, during the initial phase of water infiltration. After a certain time had elapsed, the specimen reached

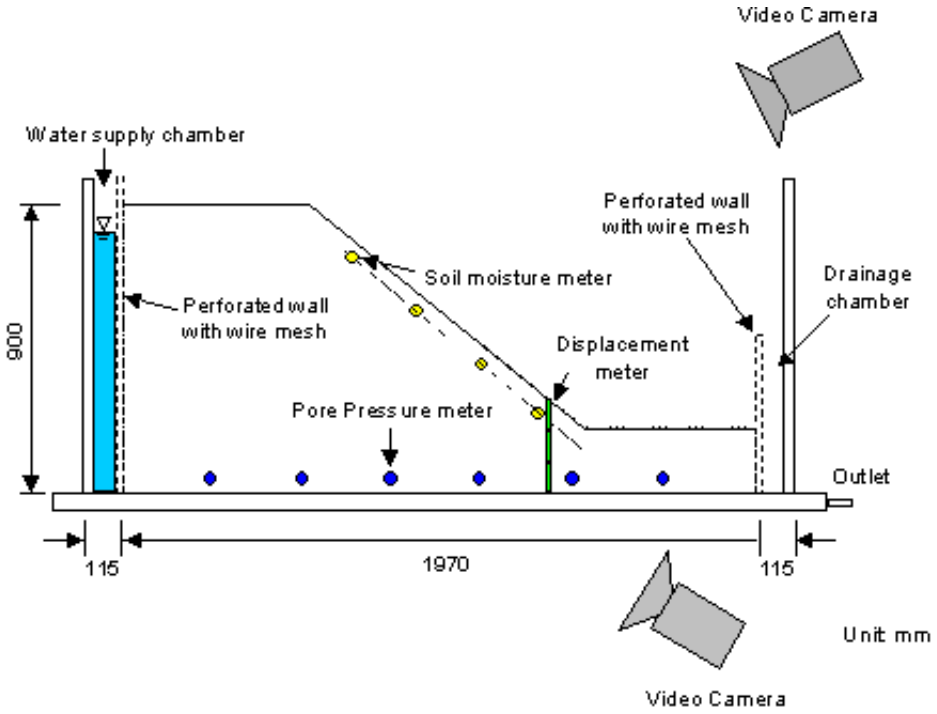

Figure 5. Schematic diagram of the soil box and the sensor locations

its yield point and axial strain increased suddenly. This point is defined as the failure initiation of the soil specimen. Once failure initiation point was reached (denoted by $\otimes$ in the figure), the development of ϵ_a progressed rapidly and large strains (>10%) were reached in relatively short time. Values of S_r when failure was induced were in the range of $90 \sim 91\%$ for all specimens. Strain rates before ($\dot{\epsilon}_1$) and after ($\dot{\epsilon}_2$) failure initiation were measured in all specimens, and it was observed that both strain rates increased as D_r decreased. This observation implies that loose soil slopes would undergo more rapid deformation than dense ones when subjected to rainfall infiltration.

Figure 6(b) shows the variation of monitored pore-water pressure inside the sample. Note that although there was negative pore-water pressure (soil suction) present within the specimen during the initial phase of water infiltration, it was not read by the miniature transducer as it could measure only positive values. In all tests, there was an increase in pressure of about $2 \sim 3$ kPa, followed by gradual decrease. Such increase may have been caused by pore-air pressure as the infiltrating water pushed up the entrapped air from the bottom portion of the specimen. Since the top end of the specimen was vented to the atmosphere, the pressure dissipated gradually.

When sufficient level of S_r was attained within the specimen, pore-water pressure started to increase and, consequently, failure was initiated within the specimen. It can be surmised from Figure 6 that the sudden increase in pore-water pressure is preceded by the reduction in initial suction within the specimen following the saturation process.

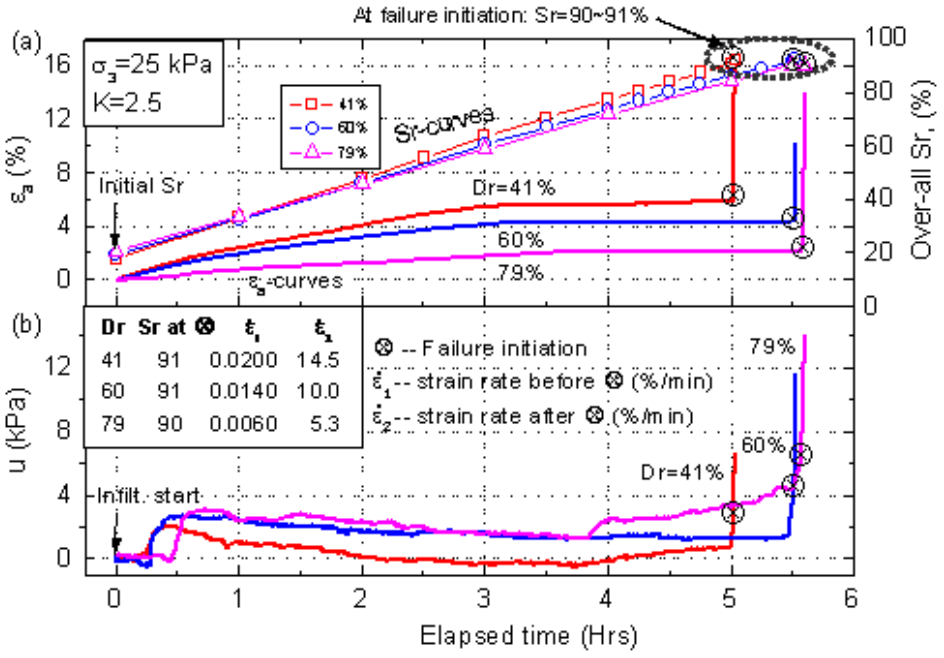

Figure 6. Time histories of: (a) axial strain, ϵ_a, and over-all degree of saturation, S_r; (b) pore water pressure, u, showing the effect of varying relative density, D_r

Results considering the effects of initial principal stress ratio K, indicative of degree of slope inclination, are shown in Figure 7. In these tests, initial D_r=60% and σ_3=25 kPa were kept constant and values of initial K were varied from 2.0 $\sim$ 3.2. As in previous case, test results showed practically bi-linear deformation time history, i.e., very small axial strains during the initial phase of water infiltration followed by rapid increase once failure initiation point was reached. Moreover, failure was induced in soil specimens at essentially constant S_r(= 91 $\sim$ 93%), irrespective of initial K. Detailed examination of Figure 7 shows that strain rates before ($\dot{\epsilon}_1$) and after ($\dot{\epsilon}_2$) failure initiation are greater for higher values of K, indicating that more rapid ground movement would be expected for steeper slopes than for mild ones. This observation is consistent with the general idea that slope gradient is a significant factor in establishing the instability state as well as the post-failure initiation condition of slopes.

4.2. Model Tests

In model tests, effects of initial relative density, D_r, slope inclination, θ, slope model shape and rainfall intensity, R, were examined. Again, due to space limitation, only two cases are presented herein. Other test results are discussed in detail by Orense et al., [16].

The model slope used in Case 1 was 70 cm high, with inclination $\theta = 40°$ and D_r=50%. Slope instability was induced by supplying water to the upslope end by maintaining 80 cm height of water in the supply chamber (see Figure 5). With the difference in pressure head between the supply chamber and the rest of the slope, water percolated into the ground.

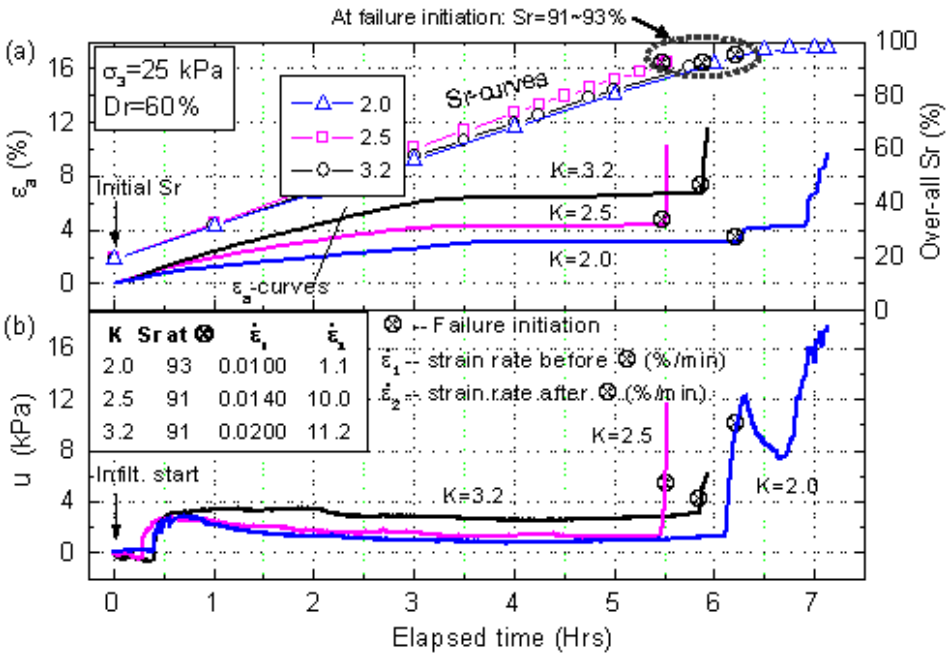

Figure 7. Time histories of: (a) axial strain, ϵ_a, and over-all degree of saturation, S_r; (b) pore water pressure, u, showing the effect of principal stress ratio, K

Figure 8 shows the monitored time histories of the lateral displacement (as monitored by the shear displacement transducer near the toe of slope and directed parallel to the the slope), volumetric water contents (defined as the ratio of the volume of water in the soil pores to the total volume) (θ_s) and pore-water pressures (PWP) at the sensor locations. The progress of wetting front (i.e., the boundary between the wetted soil and dry soil that forms during water infiltration) within the slope is indicated by the temporal development of pore-water pressure. The pore pressure readings show gradual increase in pore-water pressure, starting from the left side of the slope, consistent with the movement of the wetting front. When the region where M1 and M2 sensors were located was saturated (corresponding to S_r=90%), the ground started to deform in a very rapid manner. The maximum surface displacement near the toe was about 8 cm, while deformation 5 cm below the surface was 4 cm. This indicates that only superficial portion of the slope was involved in the movement.

Case 2 corresponds to a similar slope but with an impermeable base located 30 cm from the slope surface. For this case, instability was induced through seepage by artificial rainfall generated using hoses and nozzles set-up adjacent to the experimental box. Gauges for measuring the rainfall intensity were placed at two locations, one on the top and another at the bottom of the slope, and the accumulated rainwater was measured periodically. The monitored rainfall intensity was about $R = 42 \sim 72$ mm/hr.

Figure 9 shows the time histories of toe displacement, volumetric moisture contents and pore-water pressures. At about t=1000 sec, the infiltrating rainwater reached the soil moisture

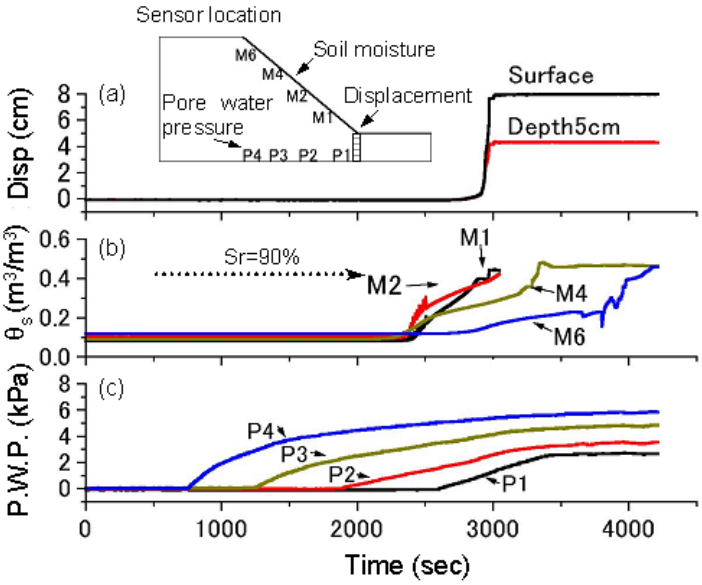

Figure 8. Time histories of: (a) toe displacement; (b) volumetric water content; (c) pore-water pressure at sensor locations (Case 1:seepage test)

transducers located 5 cm from the ground surface, and the soil moisture contents increased simultaneously. However, they remained constant as the wetting front progressed downward toward the impermeable base. As infiltration continued, a water table developed at the base of the slope, and pore-water pressure increased at P1 and P2 (at about t=5600 sec). When the water table approached M2 location, the soil moisture content at this point increased and when it registered θ_s=0.42 (equivalent to S_r=90%), the slope began to move. Displacement of about 14 cm was recorded near the toe of the slope.

In both tests, detailed examination of the movement of the surface pins recorded by video cameras revealed that small-scale slope movements (ranging from a few mm to a couple of cm) and tensile crack formation preceded the onset of failure. Cracks were formed due to the decrease in strength at the slip surface related to the pore-water pressure increase. This indicates that occurrence of such small-scale slope movements can also serve as indicator of impending slope failure.

5. PROPOSED MONITORING SCHEME

The above test results clearly demonstrated the possibility of predicting the time to failure initiation by monitoring changes in soil moisture content within the slope. Soil moisture sensors can be installed at critical locations, possibly in areas where seepage forces will develop. This can be supplemented by slope displacement monitoring (by tiltmeter, GPS-based system, etc.).

With these in mind, a simple monitoring scheme to mitigate damage to important facilities due to slope failures is proposed. First, the potential slip plane in the critical slope is assumed.

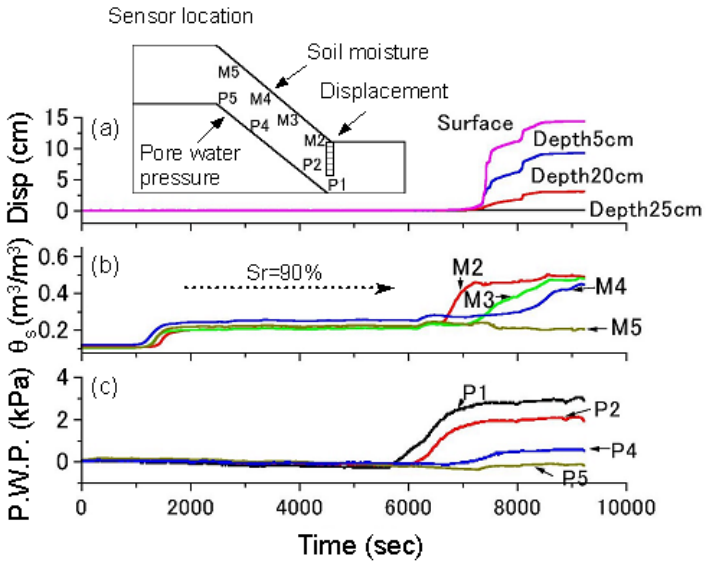

Figure 9. Time histories of: (a) toe displacement; (b) volumetric water content; and (c) pore-water pressure at sensor locations (Case 2:rainfall test)

The results of model tests indicate the inclinations of the remaining portion of the slopes after failure (defined as residual slope angle α_{res}) are the same for all cases. For Omigawa soil, it was observed from model tests that $\alpha_{res} = 20°$ (Orense et al., [16]). Thus, as shown in Figure 10(a), failure is assumed to involve the triangular region above α_{res} where soil moisture content exceeds the threshold value corresponding to the soil type present in the slope (e.g., $S_r = 90 \sim 91\%$ for Omigawa soil).

Next, the travel distance of the failed portion of the slope is estimated. For this purpose, results of field survey done by Moriwaki [17] on actual slope failures due to rainfall are used. The results, shown as black dots in Figure 10(b), showed a linear relation between the slope tangent at the source area and the ratio of slope height to travel distance. The results of all model tests are also plotted in the figure and a good agreement is observed. In using these results, the lower limit shown by the dashed line is employed to be on the safe side. Now, the slope tangent at the source area is generally known from the profile. When the travel distance, L, necessary to impact an important facility is known, the volume of slope involved in failure, which is a function of H, can be estimated. Thus, in the proposed scheme, real-time prediction not only of whether the slope will fail or not, but also the extent of the failed mass and whether it could impact a facility located downslope can be performed.

The proposed scheme is shown schematically in Figure 11. For a given rainfall data shown in Figure 11(a), moisture contents within the slope will rise, possibly starting with that near the toe (Figure 11b). From the moisture readings, the expansion of saturated region above the slip surface can be assessed in real-time and estimates of failed soil volume and the corresponding travel distance can be made (Figure 11c). When the estimated travel distance L reaches a critical value (L_{crit}) such that it would impact the facility downslope, a warning is issued. The warning is cancelled when the estimated L drops below L_{crit}.

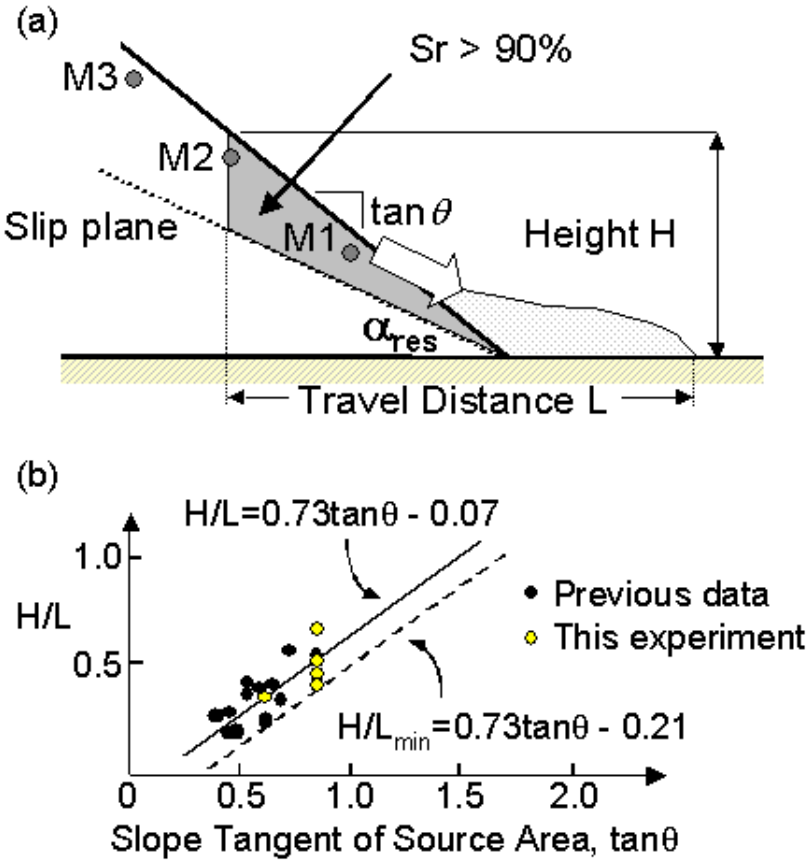

Figure 10. Basis of monitoring shceme: (a) zone with high potential to sliding, (b) relation between H/L and slope tangent of slide source area

One advantage of this method is that installation of many moisture sensors along the slope is not necessary. Monitoring can be done only at the height corresponding to L_{crit} (e.g., M3 in Figure 11). Moreover, if details of ground conditions (topography, soil properties) are known, monitoring of groundwater table and precipitation, as well as unsaturated seepage analysis and slope stability study, can be employed to supplement the assessment. Thus, a low-cost prediction system can be established. Since the system cannot predict the collapse time with high degree of accuracy, alarm can be issued several tens of minutes prior to reaching L_{crit} to give residents or transport operators sufficient time to respond.

Slope displacement monitoring is also necessary since retrogressive type of failure may occur. Furthermore, in case warning alarm is issued, it may be necessary to conduct measures such as patrolling the affected area, rescue activities and restoration works. During this period, displacement monitoring can be employed to minimize secondary damage.

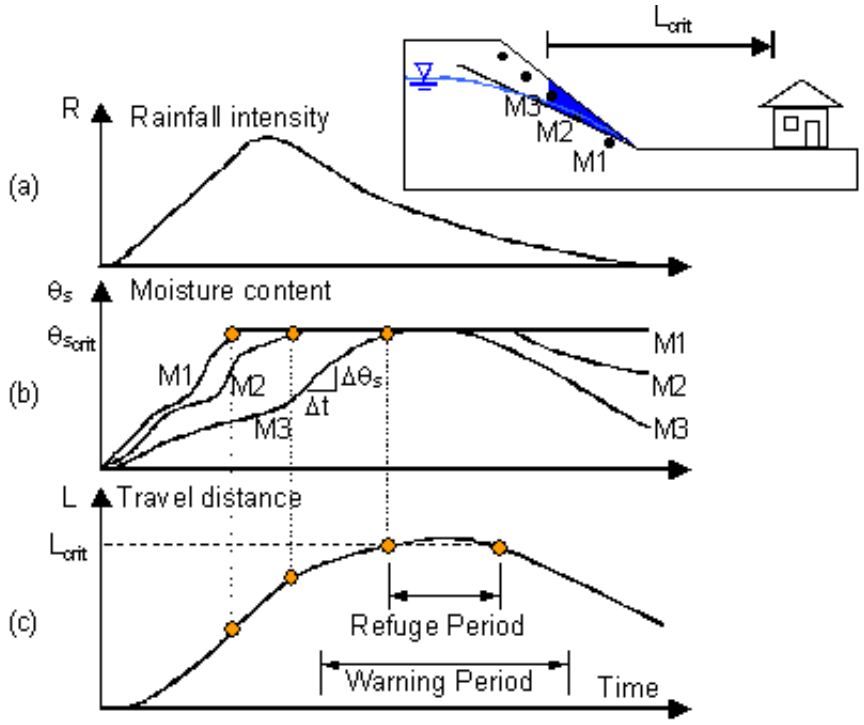

Figure 11. Schematic diagram showing the time histories of: (a) rainfall, R; (b) moisture content, θ_s; (c) travel distance, L

6. CONCLUSIONS AND RECOMMENDATIONS

Heavy rainfall due to a series of typhoons and tropical storms caused extensive damage in the coastal towns of Quezon Province. Analysis of rainfall data recorded immediately prior to the disaster, as well as comparison with historical data available, showed that the intensity of the rainfall event of 2004 was extraordinary. Other factors, such as the steepness of the slopes and presence of faults and geologic structures, were considered as contributing factors. Ocular inspections after the disaster showed that the landslides and debris flows may not have been due to logging, although it may have an impact on the scale of disaster.

Constant shear stress drained triaxial tests and seepage/rainfall tests on small-scale model slopes were performed to investigate failure initiation in sandy slopes due to rainwater infiltration. Note that the sandy materials used in the tests were obtained from a rain-induced collapsed site in Japan and are generally similar to those found in the failed slopes in Quezon, where soils are sandy silt to silty sand in nature.

In all element tests, failure in the specimen was initiated due to the development of pore water pressure within the specimen. During rainfall, soil suction would dissipate as a result of saturation of soil profile and failure would take place due to the development of pore water pressure. The strain rate after failure initiation, , decreases with increasing relative density, suggesting that looser deposits would undergo more rapid movement during failure than dense

ones. For the same initial relative density and water infiltration rate, increasing initial K increases the strain rates before ($\dot{\epsilon}_1$) and after ($\dot{\epsilon}_2$) failure initiation, indicating that steeper slopes would experience faster deformation during rain-induced slope failure than gentler slopes.

Seepage and rainfall tests on model slopes indicate that slope failure always occurred when the soil moisture content within a certain region near the toe of slope became nearly fully saturated, even if other parts of the sliding mass were still only partially saturated. The threshold value of volumetric water content required for failure to occur in Omigawa sand slope with D_r=50% was θ_s=0.42-0.43, corresponding to S_r=90-91%. Once failure was initiated at the toe of slope, the unstable zone propagated upward to other portions of the slope. When the entire slope was under a high degree of saturation, rapid propagation of failure occurred. Minor slope displacements, such as surficial movements in the range of a few cm, were recorded prior to rapid failure. In some cases, these were accompanied by formation of cracks upslope.

Both element tests and model tests showed that as the soil moisture contents approached saturated values, ground deformations were mobilized. This observation strongly indicates that prediction of slope failure initiation is possible by monitoring changes in soil moisture contents and displacement within the slope.

From these results, a simple methodology was proposed to predict in real-time the occurrence of rainfall-induced failures in sandy slopes by carefully monitoring changes in soil moisture contents and deformations at critical locations within the slope. Then, appropriate warning can be issued to mitigate damage to facilities downslope. Further investigations by numerical analyses and/or actual in-situ monitoring are necessary to validate the proposed system.

ACKNOWLEDGEMENTS

The laboratory tests presented in this paper were performed with the cooperation of Messrs. K. Farooq, S. Shimoma, T. Honda and K. Maeda of Geotechnical Engineering Laboratory, University of Tokyo. Sampling at Omigawa slope was made possible with the assistance of Mr. K. Ono from Chiba Prefecture Public Works office and Dr. Y. Tsukamoto of Tokyo Science University. Helpful comments were provided by Prof. I. Towhata of University of Tokyo. A part of this research was conducted under the auspices of the Disaster Mitigation Engineering for Transport Infrastructures (JR-East Endowed Chair) while the author served as Visiting Associate Professor at the University of Tokyo. Reconnaissance work in the Quezon Province was performed with the assistance of Engr. S. Sapuay of Infra-tech Consultants and Dr. E. Billedo of DENR Mines and Geosciences Bureau. Moreover, the overall cooperation of Mayor F. America of Infanta, Quezon, Prof. J. Foronda of the University of the Philippines, Mr. E. Esguerra of ERE Consulting, Mr. N. Resplandor of Infanta Congressman's Office, and Engr. E. Morales was very helpful. The author would like to extend his gratitude to JR-East, DENR-MGB and the above mentioned individuals.

REFERENCES

1. E. W. Brand, J. Premchitt and H.B. Phillipson *Relationship between rainfall and landslides in Hong Kong* Proceedings of the 4th International Symposium on Landslides, Ontario, Canada, 377-384 (1984)

2. D.K. Keefer, R.C. Wilson, R.K. Mark, E.E. Brabb, W.M. Brown III, S.D. Ellen, E.L. Harp, G.F. Wieczorek, C.S. Alger and R.S. Zatkin, *Real-time landslide warning during heavy rainfall*, Science, No. 238, 921-925 (1987)
3. R.C. Wilson, J.D. Torikai and S.D. Ellen, *Development of rainfall warning threshold for debris flows in Honolulu District, Oahu*, U. S. Geological Survey Open-file Report, Washington, D.C. 92-521 (1992)
4. K. Okada, and T. Sugiyama, *Prediction of slope failure by critical rainfall in railway and its application*, Tsuchi-to-Kiso, Vol. 49, No. 7, 22-24, in Japanese (2001)
5. Office for Coordination of Humanitarian Affairs, Philippine floods: OCHA Situation Report No. 4. http://www.reliefweb.int
6. R.P. Orense, S.E. Sapuay and E.B. Billedo, *Characteristics of the 2004 sediment-related disasters in Quezon Province, Philippines triggered by tropical cyclones*, Journal of Natural Disaster Science, submitted for publication (2005)
7. M. Fukuoka, *Landslides associated with rainfall*, Geotechnical Engineering, Vol. 11, 1-29 (1980)
8. Chiba Prefecture, Civil & River Division, *Report of Disaster in Chiba caused by Autumn Rain Front of September 6-7, 1971 and Typhoon No. 25*, in Japanese (1972)
9. K.A. Johnson and N. Sitar, *Hydrologic conditions leading to debris flow initiation*, Canadian Geotechnical Journal, Vol. 27, No. 6, 789-801 (1990)
10. N. Sitar, S.A. Anderson and K.A. Johnson, *Conditions leading to the initiation of rainfall-induced debris flows*, Geotechnical Engineering Division, Specialty Conference on Stability and Performance of Slopes and Embankments-II, ASCE, New York, N. Y., 834-839 (1992)
11. J.D. Eckersley, *Instrumented laboratory flowslides*, Geotechnique, Vol. 40, No. 3, 489-502 (1990)
12. E.W. Brand, *Some thoughts on rain-induced slope failures*, Proceedings of the 10th International Conference on Soil Mechanics and Foundation Engineering, Stockholm, Vol. 3, 373-376 (1981)
13. R.P. Brenner, H.K. Tam and E.W. Brand, *Field stress path simulation of rain-induced slope failure*, Proceedings of the 11th International Conference on Soil Mechanics and Foundation Engineering, San Francisco, Vol. 2, 991-996 (1985)
14. K. Farooq, R.P. Orense and I. Towhata, *Response of unsaturated sandy soils under constant shear stress drained condition*, Soils and Foundations, Vol. 44, No. 2, 1-13 (2004)
15. S. Shimoma, R.P. Orense, T. Honda, K. Maeda and I. Towhata, *Model tests on slope failures caused by heavy rainfall*, Proceedings, Interpraevent2002 in the Pacific Rim International Congress, Nagano, Japan, Vol. 2, 547-557, (2002)
16. R.P. Orense, S. Shimoma, K. Maeda. and I. Towhata, *Instrumented slope failure due to water seepage*, Journal of Natural Disaster Science, Vol. 26, No. 1, 15-26 (2004).
17. H. Moriwaki, *Prediction of distance attained by failed slopes*, Landslides, Vol. 24, No. 2, 10-16, in Japanese (1987)

APPENDIX

NOMENCLATURE

Symbol description

D_r	initial relative density (%)
H	slope height (m)
K	principal stress ratio
L	travel distance of landslide (m)
R	rainfall (mm/hr)
Q	infiltration rate (cm^3/hr)
S_r	degree of saturation (%)
t	time (sec)
u	pore-water pressure (kPa)
w	initial moisture content (%)
α_{res}	resodual slope angle (°)
ϵ_a	axial strain(%)
$\dot{\epsilon_1}$	axial strain rate before failure initiation(%/min)
$\dot{\epsilon_2}$	axial strain rate after failure initiation (%/min)
σ_n	(kPa)
σ_1	(kPa)
σ_3	(kPa)
θ	slope angle (°)
θ_s	volumetric water content (%)
τ	shear stress(kPa)

Subscript and abbreviation

crit	subscript refer to critical value
PWP	pore water pressure

